A Novel Non-photochemical Quenching Mechanism of LHCII at High-temperature

Meixia Ruan[1†], Tengfei Ma[2†], Guohong Liao[1,3], Heyuan Liu[1], Meijiao Wang[1], Fang Jiao[1,3], Zhuan Wang[1], Hailong Chen[1,3,6], Yingjie Wang[4*], Wei Ding[1,3*], Weimin Liu[2*], Yuxiang Weng[1,3,6*]

Author affiliations:

[1]Beijing National Laboratory for Condensed Matter Physics, Institute of Physics, Chinese Academy of Sciences, Beijing 100190, China;

[2]School of Physical Science and Technology, ShanghaiTech University, Shanghai 201210, China;

[3]University of Chinese Academy of Sciences, Beijing 100049, China;

[4]Institute of Systems and Physical Biology, Shenzhen Bay Laboratory, Shenzhen 518000, China

[5]Department of Chemistry and Supercomputing Institute, University of Minnesota, Minneapolis, MN, USA

[6]Songshan Lake Materials Laboratory, Dongguan, Guangdong, China.

[†]These authors contributed equally

[*]Corresponding authors:

Yuxiang Weng (Email: yxweng@iphy.ac.cn); Weimin Liu (Email: liuwm@shanghaitech.edu.cn);

Wei Ding (Email: dingwei@iphy.ac.cn); Yingjie Wang (Email: wangyj@szbl.ac.cn)

Supplementary Information

FSRS kinetic fitting model

A multi-exponential decay kinetic for a set of discrete rate constants k_i with individual initial contribution a_i can be expressed as,

$$\mathrm{I(t)} = \sum_{i=1}^{n} a_i e^{-k_i t} \tag{1}$$

which has been extensively applied in kinetic analyses. For clarity, the convolution operation with the IRF is omitted in all subsequent equations.

When the system exhibits conformational or structural heterogeneity on the potential energy surface, k_i can change from discrete values to continuous distributed function, and the corresponding finite set of discrete lifetimes is insufficient to accurately describe the system's kinetics. To overcome this limitation, the discrete lifetime distribution is extended to a continuous form that accounts for the intrinsic structural heterogeneity of the sample[1]. Within the Laplace transform formalism, the model is expressed as:

$$I(t) = \int_{\tau_{lower}}^{\tau_{upper}} \rho(\tau) e^{\frac{-t}{\tau}} d\tau \tag{2}$$

Where $\rho(\tau)$ is the continuous lifetime distribution function, determined by the intrinsic properties of the system, spanning the lifetime interval $[\tau_{lower}, \tau_{upper}]$. Accordingly, the fitting objective shifts from determining discrete lifetimes τ and their pre-exponential factors a_i to resolving the continuous lifetime distribution $\rho(\tau)$ within the specified interval.

In practice, the finite temporal resolution of the FSRS experiment, defined by its instrument response function (IRF), precludes direct reconstruction of a perfectly continuous lifetime distribution. Therefore, a discrete approximation of the integral is adopted. The lifetime domain is divided into finite differential intervals of width $\Delta\tau$, matched to the experimental IRF, yielding the following expression:

$$\mathrm{I(t)} = \int_{\tau_{lower}}^{\tau_{upper}} \rho(\tau) e^{\frac{-t}{\tau}} d\tau \approx \sum_{i=1}^{n} \rho(\tau_i) e^{\frac{-t}{\tau_i}} \Delta\tau \tag{3}$$

In the present FSRS experiment, the IRF was determined to be ~70 fs. Accordingly, the lifetime sampling precision $\Delta\tau$ was set to 100 fs, and the lower boundary of the lifetime distribution interval was defined as 100 fs to match the experimental time resolution. The excitation energy transfer from chlorophyll (Chl) to lutein (Lut) in LHCII system was studied, where the donor (Chl) transfers the excitation energy to the acceptor (Lut) with a time constant τ_D, the excited state of the acceptor is populated then undergoes subsequent relaxation with a time constant τ_A, the system satisfies the following rate equation:

$$\frac{dn_D}{dt} = -\frac{n_D}{\tau_D} \tag{4}$$

$$\frac{dn_A}{dt} = \frac{n_D}{\tau_D} - \frac{n_A}{\tau_A} \tag{5}$$

n_D represents the population of donor (Chl), and n_A represents the population of accepter (Lut). Equation (6) shows the kinetic of Lut population.

$$n_A(t) = \frac{n_D(0)\tau_A}{\tau_D - \tau_A}\left(e^{\frac{-t}{\tau_D}} - e^{\frac{-t}{\tau_A}}\right) = \frac{\tau_A}{\tau_D - \tau_A}\left(e^{\frac{-t}{\tau_D}} - e^{\frac{-t}{\tau_A}}\right) \tag{6}$$

For simplicity, the initial population of the Chl excited state is set as of $n_D(0) = 1$. Specifically, as an acceptor, the decay lifetime of Lut is a constant set as τ_A=15 ps, irrespective of any conformational states. In contrast, the energy transfer time τ_D from Chl to Lut is strongly dependent on the conformation of the LHCII, since according to the Dexter energy transfer equation[2], τ_D is sensitive to the Lut-Chl distance. When $\tau_D < \tau_A$, the kinetic trace of Lut showcases a rapid population with time constant τ_D, followed by relaxation with τ_A. When $\tau_D > \tau_A$ (Extended Data Fig.1), the kinetic trace exhibits a rise corresponding to the relaxation of the acceptor, while the decay represents the slower population progress from the donor[3]. This counter intuitive temporal behavior is referred to as inverted kinetics[3,4].

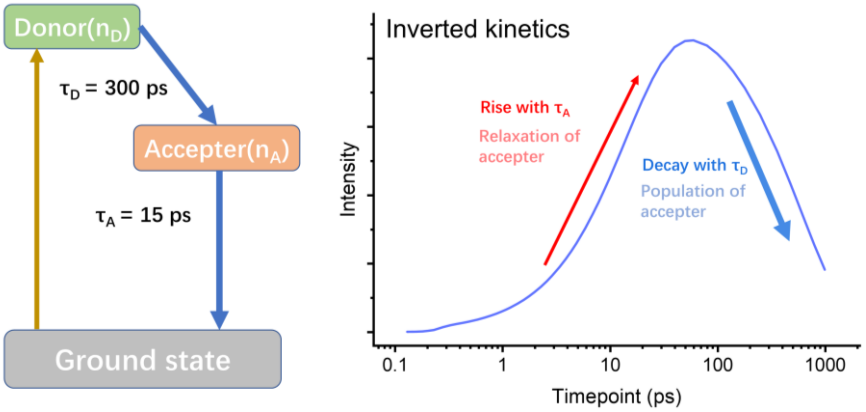

Extended Data Fig. 1: Schematic of inverted kinetics.

MD simulations reveal that Lut1-Chl612 distance exists a 1-2 Å distribution[5-7]. This heterogeneity modulates the electronic coupling strength between two pigments, thereby giving rise to a corresponding distribution of energy transfer rates (τ_D). To quantitatively capture this distributed kinetic behavior, we employed the continuous lifetime distribution model described above, which incorporates the coupled donor–acceptor population dynamics. Within this framework, the kinetic evolution of lutein can be expressed as follows:

$$\mathrm{I(t)} = \sum_{i=1}^{n} \frac{\rho(\tau_{D_i})\Delta\tau_D\tau_A}{\tau_{D_i} - \tau_A}\left(e^{\frac{t_0-t}{\tau_{D_i}}} - e^{\frac{t_0-t}{\tau_A}}\right) \quad (7)$$

Where τ_{D_i} represent the lifetime of Chl to Lut energy transfer, τ_A represents the decay lifetime of Lut (15 ps). The lifetime τ_{D_i} exhibits a distribution of energy transfer lifetime, the fastest component τ_{D_1} = 100 fs, which is potentially even shorter and is limited by the IRF of FSRS experiment, and the slowest component τ_{D_n} extending up to hundreds of picoseconds, ultimately constrained by the Chl excited state lifetime.

Considering the entire Chl-Lut energy transfer processes observed in FSRS comprise both the normal kinetic ($\tau_{D_i} < \tau_A$) and the inverted kinetic ($\tau_{D_i} > \tau_A$), we separate the kinetic signal into the normal (I_N) and inverted (I_I) parts:

$$I(t) = I_N(t) + I_I(t) \quad (8)$$

For the inverted kinetic (τ_{D_i}> 15 ps), due to the limited temporal detection window of ~100 ps, within this window, the long-lived components are only represented by sparse data points; it is impractical to resolve the

energy transfer time beyond nanosecond. Therefore, instead of modeling a continuous distribution of τ_{D_i}, we employed an average lifetime 300 ps to capture the collective contribution of all energy transfer lifetimes in the inverted kinetic. The amplitude A_{avg}, associated with this τ_{avg}=300 ps average lifetime, represents the integrated contribution of the long-lived (invert) component.

$$I_I(\mathrm{t}) = A_{avg}\left(e^{\frac{t_0-t}{\tau_{avg}}} - e^{\frac{t_0-t}{\tau_A}}\right), A_{avg} > 0 \quad (9)$$

For the normal kinetic component ($I_N(t)$), corresponding to the Chl to Lut energy transfer regime where $\tau_{D_i} < \tau_A$=15 ps, the lifetime range is defined as from 0.1 to 15 ps. With a step size $\Delta\tau_D = 100$ fs, this range is discretized into 149 equally spaced intervals, corresponding to 149 sampling points of the lifetime distribution $\rho(\tau)$. Directly fitting such a large number of parameters, we take guidance from molecular dynamics (MD) simulations,[5,8,9] which reveal a Gaussian-like conformational distribution of Lut. Accordingly, we approximate the lifetime distribution function $\rho(\tau)$ by Gaussian function characterized by only two free parameters: the Gaussian center τ_c and width *w*. Under this treatment, the kinetic contribution of the component I_N is expressed as:

$$I_N(t) = \sum_{i=1}^{n} \frac{\rho(\tau_{D_i})\Delta\tau_D\tau_A}{\tau_{D_i} - \tau_A}\left(e^{\frac{t_0-t}{\tau_{D_i}}} - e^{\frac{t_0-t}{\tau_A}}\right), \qquad \rho(\tau) = e^{\frac{-(\tau-\tau_c)^2}{w^2}}$$

The overall excited state dynamics of Lut, incorporating both the normal and (averaged) invert components, can then be described as:

$$\mathrm{I(t)} = \sum_{i=1}^{n} \frac{\rho(\tau_{D_i})\Delta\tau_D\tau_A}{\tau_{D_i} - \tau_A}\left(e^{\frac{t_0-t}{\tau_{D_i}}} - e^{\frac{t_0-t}{\tau_A}}\right) + A_{avg}\left(e^{\frac{t_0-t}{\tau_{avg}}} - e^{\frac{t_0-t}{\tau_A}}\right), \ \rho(\tau) = e^{\frac{-(\tau-\tau_c)^2}{w^2}}$$

Where $\Delta\tau_D$ = 0.1 ps, $A_{avg} > 0$, 0.1ps $\leq \tau_{D_i} <$ 15 ps for normal kinetic components, and $\tau_D >$ 15 ps for inverted kinetics. The relative contribution weights for the normal kinetics and the inverted kinetics can be evaluated by calculate their pre-exponential factors as $\sum_{i=1}^{n} \frac{\rho(\tau_{D_i})\Delta\tau_D\tau_A}{\tau_{D_i}-\tau_A}$ and $A_{avg.}$

In order to simplify the fitting model, the pre-exponential factors of I_D was normalized as $\sum_{i=1}^{n} \frac{\rho(\tau_{D_i})\Delta\tau_D\tau_A}{\tau_{D_i}-\tau_A} = 1$. Therefore, the relative contribution of the slow inverted kinetic component W_{slow} can be described as:

$$W_{slow} = \frac{A_{avg}}{\sum_{i=1}^{n} \frac{\rho(\tau_{D_i})\Delta\tau_D\tau_A}{\tau_{D_i} - \tau_A} + A_{avg}} = \frac{A_{avg}}{1 + A_{avg}}$$

Based on the above analysis, we have established a kinetic model employing a continuous lifetime distribution to describe the excited state dynamics of Lut within LHCII. This model introduces three key fitting parameters: the Gaussian center τ_c, distribution width w, and the proportion of long-lived component A_{avg}. The developed model was employed to fit the excited-state kinetic traces of Lut acquired via FSRS at varied temperatures, the FSRS dynamics and fitting results are shown in Fig. 3 and Extended Data Fig. 2.

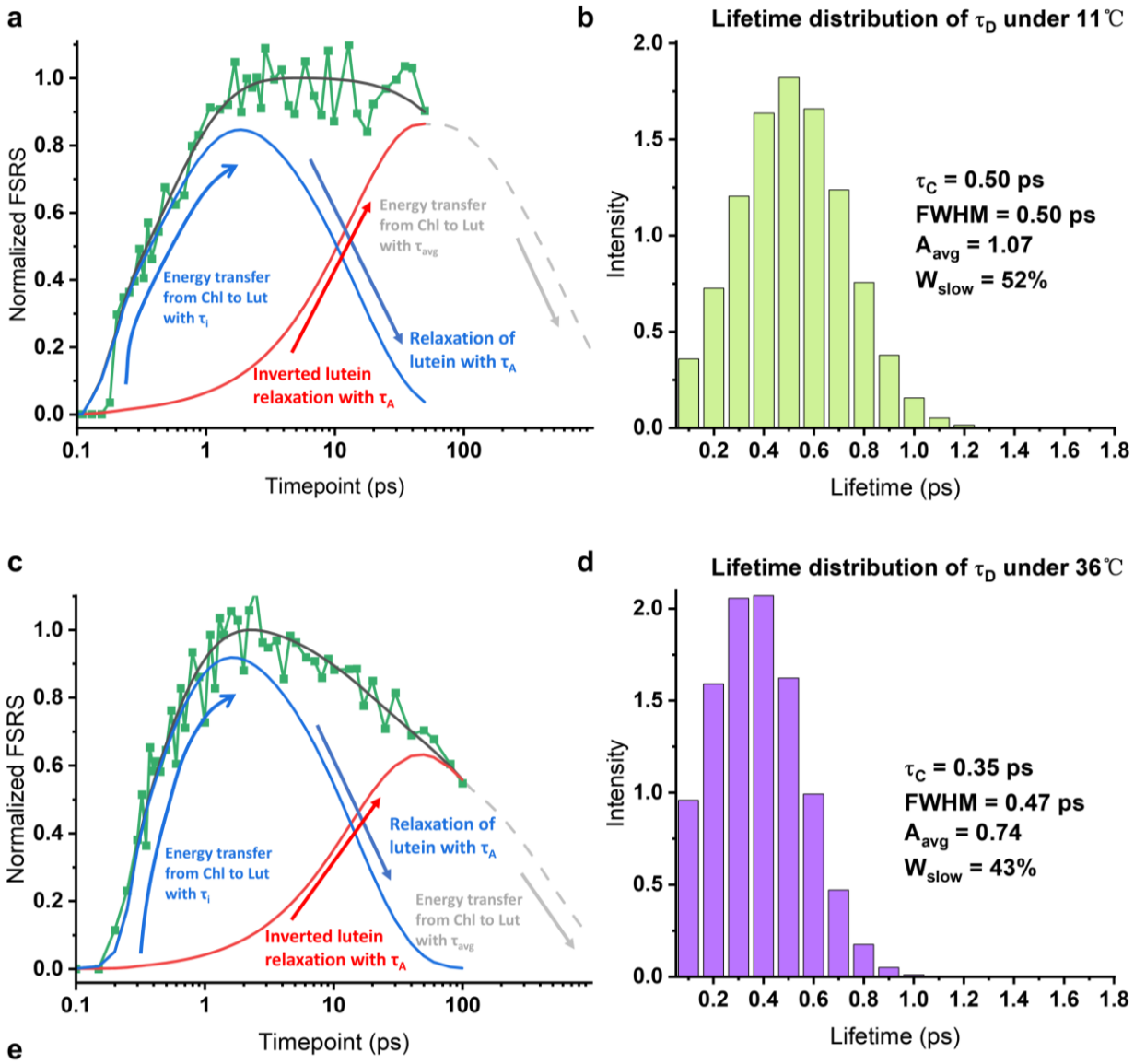

e

Temperature	11 ℃	25 ℃	36 ℃	55 ℃
τ_C (ps)	0.50	0.50	0.35	0.10
FWHM (ps)	0.50	0.41	0.47	0.47
A_{avg}	1.07	1.10	0.74	0.44
W_{slow}	52%	52%	43%	31%

Extended Data Fig. 2: FSRS dynamics and fitting result under varied temperatures. FSRS dynamics and the fits at 11 ℃ (a) and 36 ℃(c), the blue traces in left panels represent the normal kinetics I_N component, and the red trace denotes the inverted kinetics I_I component. Lifetime distribution for the rising phases at 1770 cm^{-1} under 11 ℃ (b) and 36 ℃(d). (e) The fitting parameters at different temperatures.

The fitting results reveal two distinct kinetic regimes. (1) I_N (t) component (blue fitted kinetic trace): This component exhibits a rapid population rise described by a continuous distribution of transfer lifetimes and subsequently decays with a characteristic lifetime of 15 ps, corresponding to the relaxation of the lutein S_1 state. (2) I_I (t)component (red fitted kinetic trace): This kinetic trace rises with 15 ps lifetime and decays with long time τ_{avg}=300 ps. In this invert kinetic regime, the rising phase corresponds to the relaxation of the Lut

S_1 state, while the subsequent decay phase reflects the long-lived energy transfer process from Chl to Lut. The relative contribution weight for the fast and low EET at 25 ℃ is 52% and 48%. As shown in Extend data Table 1, the fitting τ_c are identical 0.50 ps for LHCII under 11 ℃ and 25 ℃, with only minor changes in full width at half maxima (FWHM) and A_{avg}. Upon heating to 36 ℃ and 55 ℃, τ_c progressively decreases to 0.35 ps and 0.10 ps, respectively, while FWHM remain at 0.47 ps at high temperature, the long-time amplitude A_{avg} drop from 1.10 (25 ℃) to 0.74 and 0.44, indicating accelerated Chl to Lut energy transfer. The pronounced reduction of A_{avg} and W_{slow} suggest a diminished contribution from weakly coupled Chl-Lut pairs, consistent with a more compact and dynamically quenched configuration at high temperature.

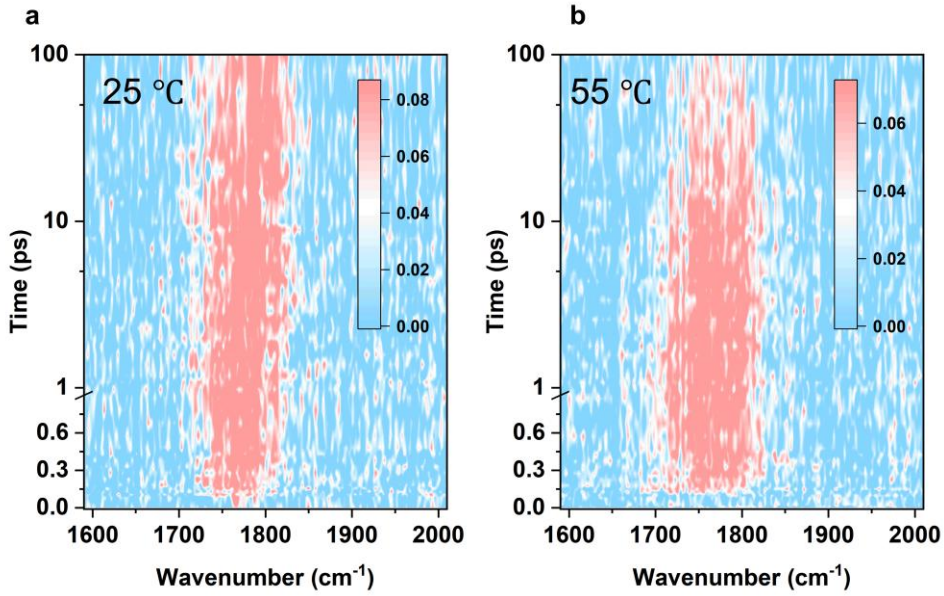

Extended Data Fig. 3: 2D contour plots of the FSRS signals from LHCII under 680 nm actinic pump at 25 ℃ (a) and 55 ℃ (b).

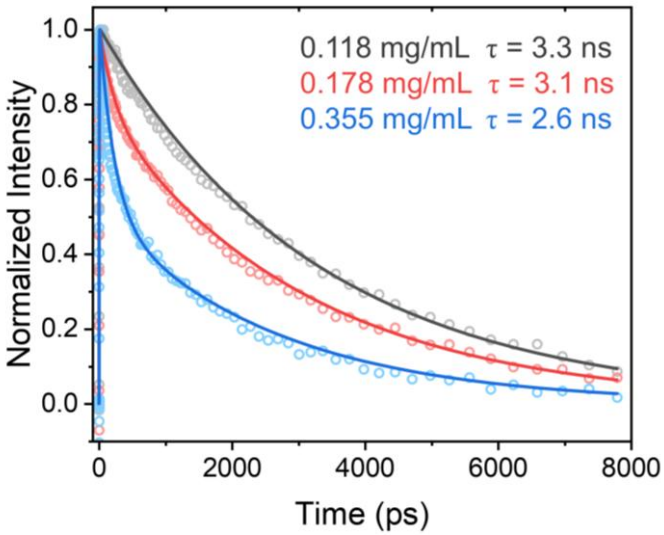

Extended Data Fig. 4: Transient absorption kinetic at 690 nm of LHCII at varied protein concentration, excited at 480 nm.

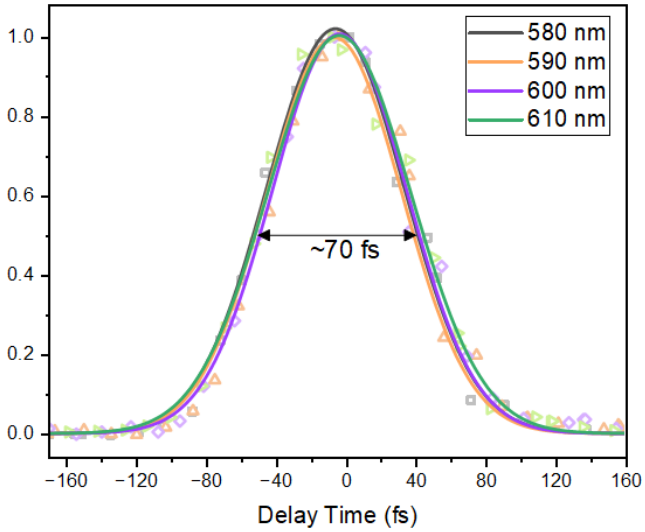

Extended Data Fig. 5: The instrument response function (IRF) of FSRS at the selected Raman probe wavelengths and fitted curve by Gaussian function (solid lines).

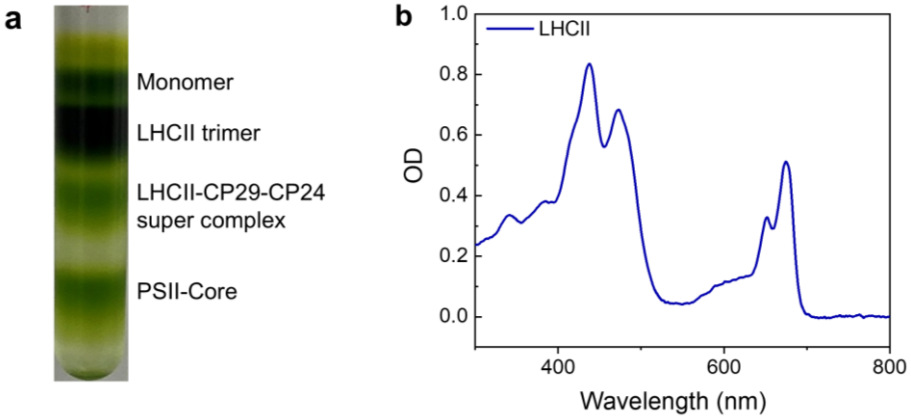

Extended Data Fig. 6: LHCII purification and absorption spectrum. (a) Sucrose density gradient ultra-centrifugation separation result of LHCII trimer. (b) UV-vis absorption spectra of LHCII trimer.

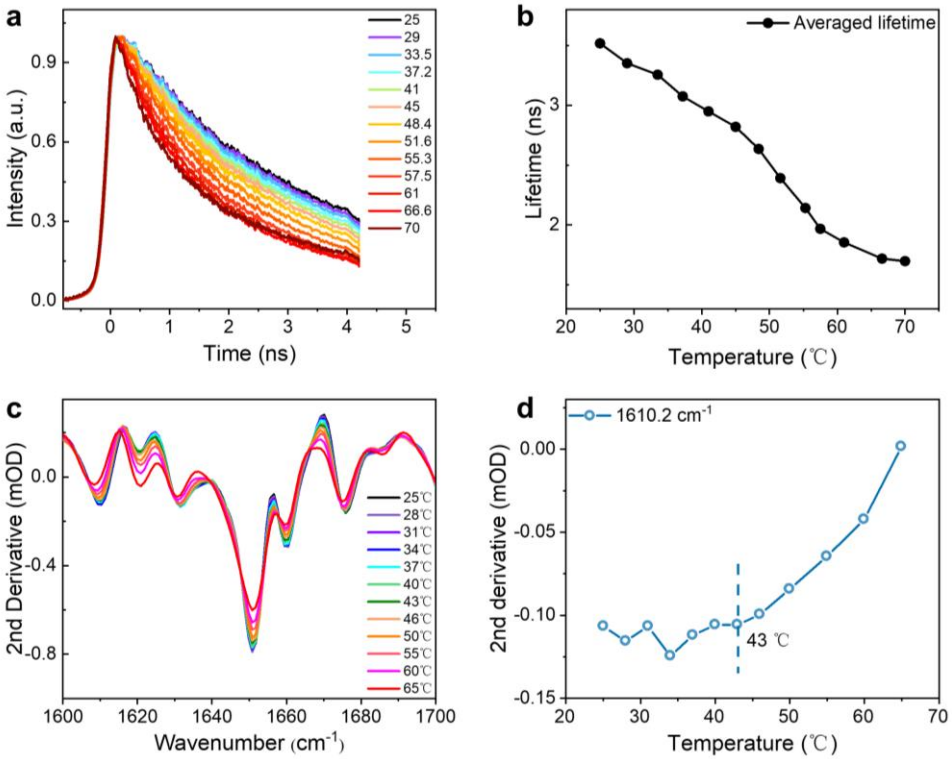

Extended Data Fig. 7: Time-resolved fluorescence spectra and TFIR spectra of LHCII trimer at varied temperatures. (a) Fluorescence decay kinetics of LHCII at different temperatures. (b) Averaged fluorescence lifetime of LHCII using bi-exponential fitting, the averaged lifetime is calculated as $t_1*A_1+t_2*A_2$, wherer A is the corresponding pre-exponential factor. (c) Secondary derivative FTIR spectra of LHCII trimer (0.03% DDM, pH 7.8) under varied temperatures from 25 ℃ to 65 ℃. (d) Thermal titration of the signal at 1610.2 cm^{-1}, which is characteristic of the formation of specific LHCII network stabilized by the intertrimer hydrogen bonds, the dash line at 43 ℃ shows the turning point.

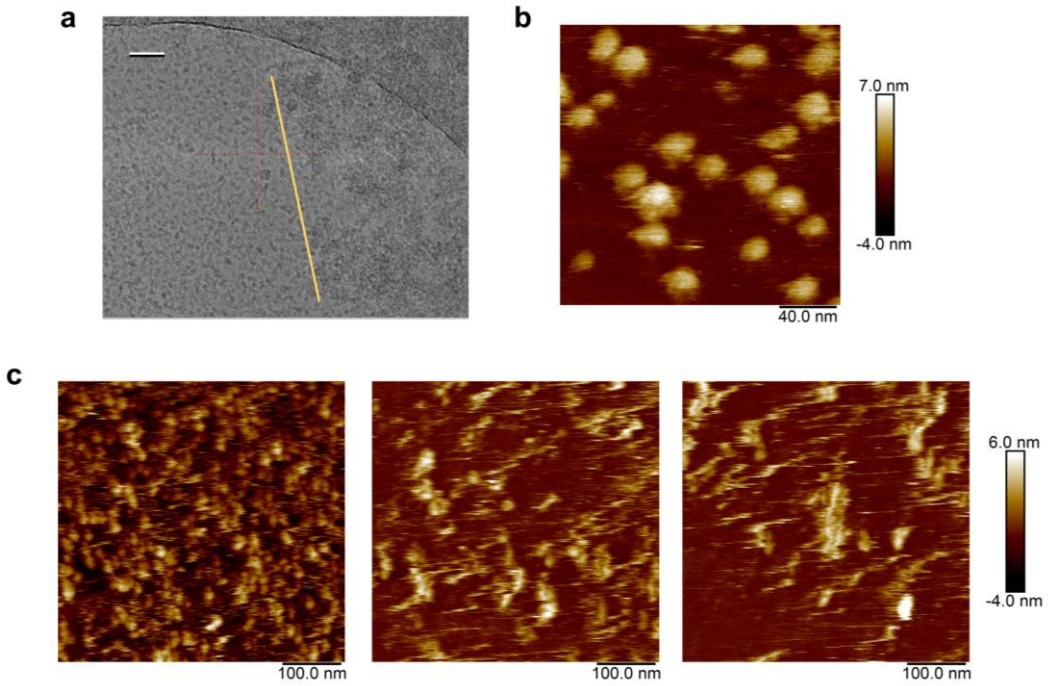

Extended Data Fig. 8: AFM and 200 kV cryo-EM images of LHCII trimer at elevated temperature. (a) 200 kV cryo-EM images of LHCII trimer, showing the aggregation of LHCII, the yellow line defines the edges of the non-aggregated and aggregated samples. The scale bar is 50 nm. (b) AFM image of LHCII at room temperature. (c) In situ AFM images at 43°C, showing gradual aggregation of LHCII trimer. From left to right are 0, 55 and 87 minutes respectively.

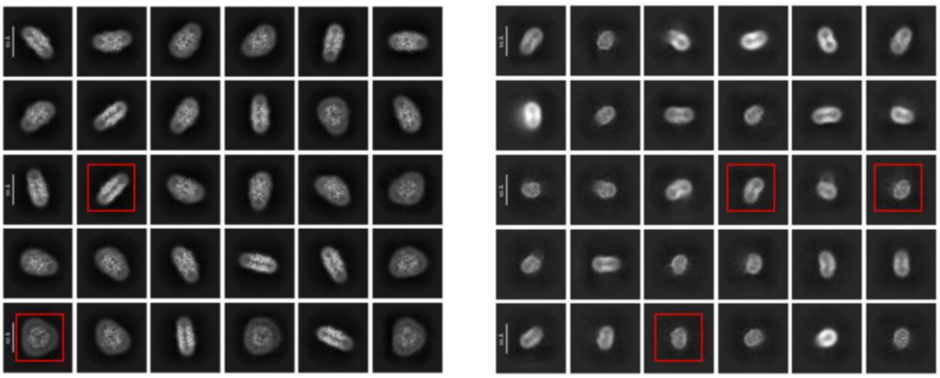

Extended Data Fig. 9: The 2D views of the further processed (left) and detergent-loss smaller (right) particles at 55 °C. The red boxes provide an intuitive sight of size difference. This indicates that detachment of detergent molecules from LHCII trimer at high temperature leads to aggregation.

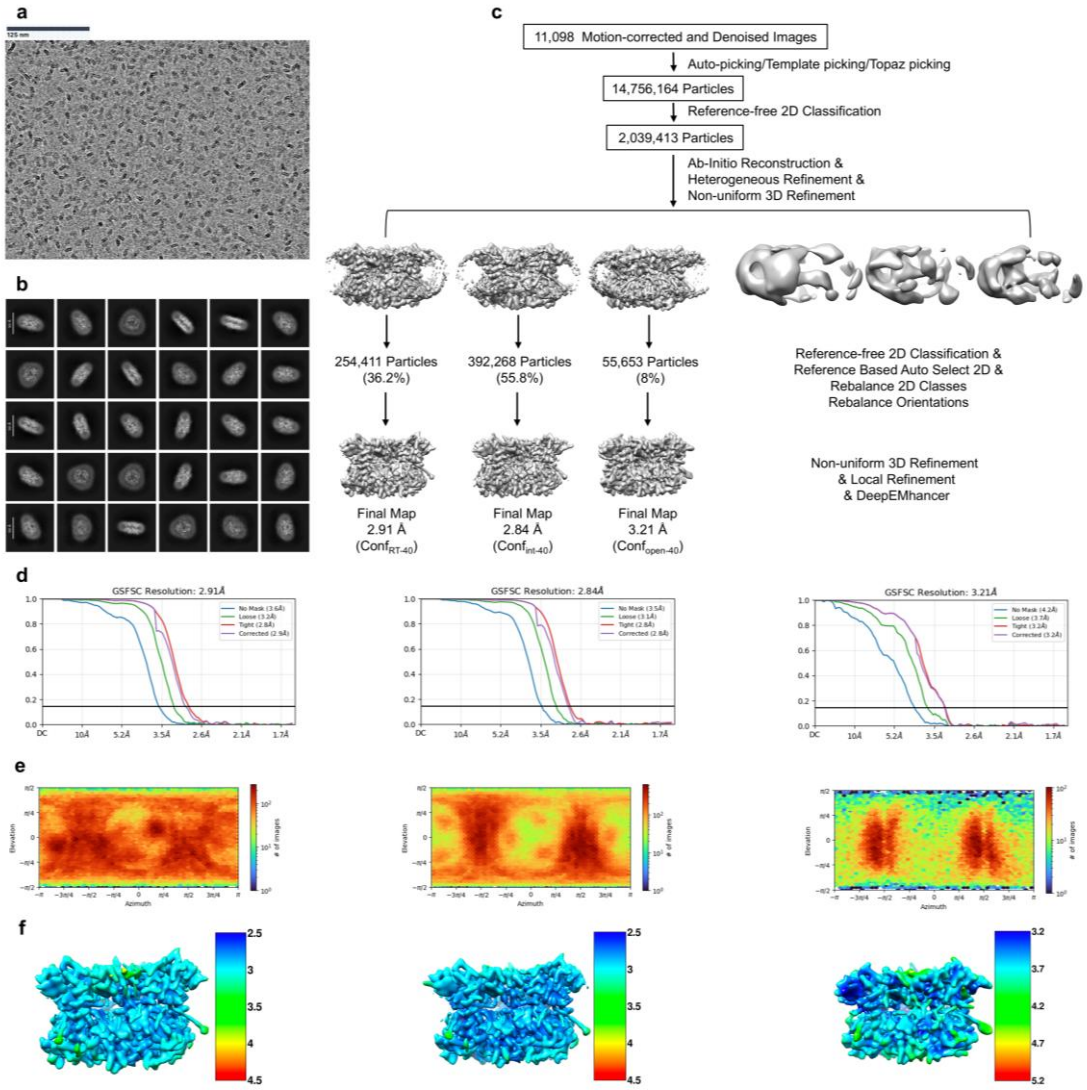

Extended Data Fig. 10: Structural analysis flow chart of LHCII at 40 °C. a. A representative cryo-EM image of 11,098 collected. **b.** 2D class averages of characteristic projection views of cryo-EM particles selected for further processing, a 125 nm scale bar is given. **c.** Flowchart for cryo-EM data processing. **d.** Gold-standard Fourier Shell Correlation (FSC) curves of three conformations respectively, the 0.143 cut-off value is indicated by a horizontal black line. **e.** Angular distribution plot of particles used for final 3D refinement. The distribution was calculated with cryoSPARC v.4.7.1. The different colors indicate the different number of particles that have such orientations according to the bar shown on the right. **f.** Local resolution map analyzed by the local resolution estimation tool in cryoSPARC.

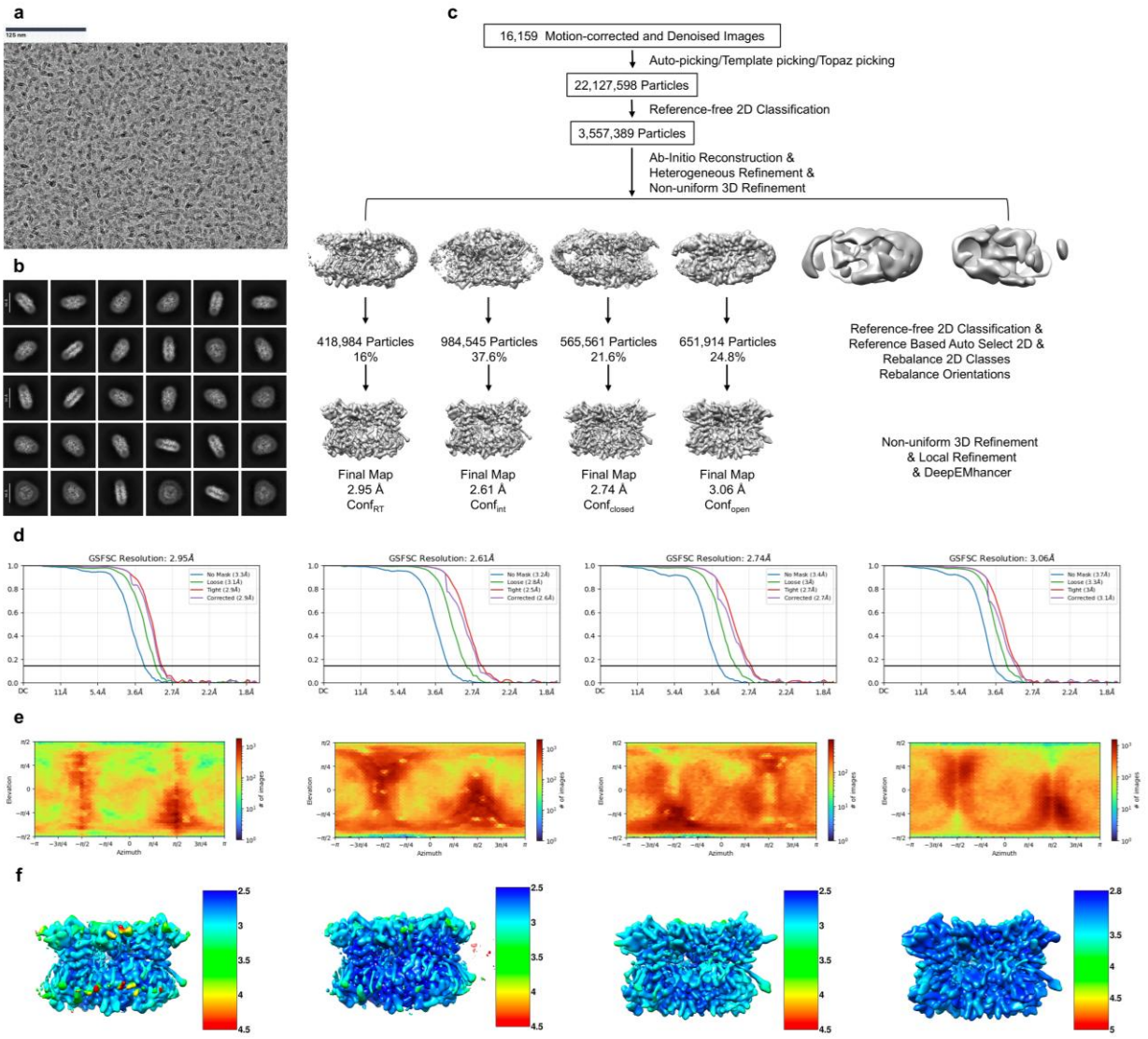

Extended Data Fig. 11: Structural analysis flow chart of LHCII at 55 °C. a. A representative cryo-EM image of 16,159 collected. **b.** 2D class averages of characteristic projection views of cryo-EM particles selected for further processing, a 125 nm scale bar is given. **c.** Flowchart for cryo-EM data processing. **d.** Gold-standard Fourier Shell Correlation (FSC) curves of three conformations respectively, the 0.143 cut-off value is indicated by a horizontal black line. **e.** Angular distribution plot of particles used for final 3D refinement. The distribution was calculated with cryoSPARC v.4.7.1. The different colors indicate the different number of particles that have such orientations according to the bar shown on the right. **f.** Local resolution map analyzed by the local resolution estimation tool in cryoSPARC.

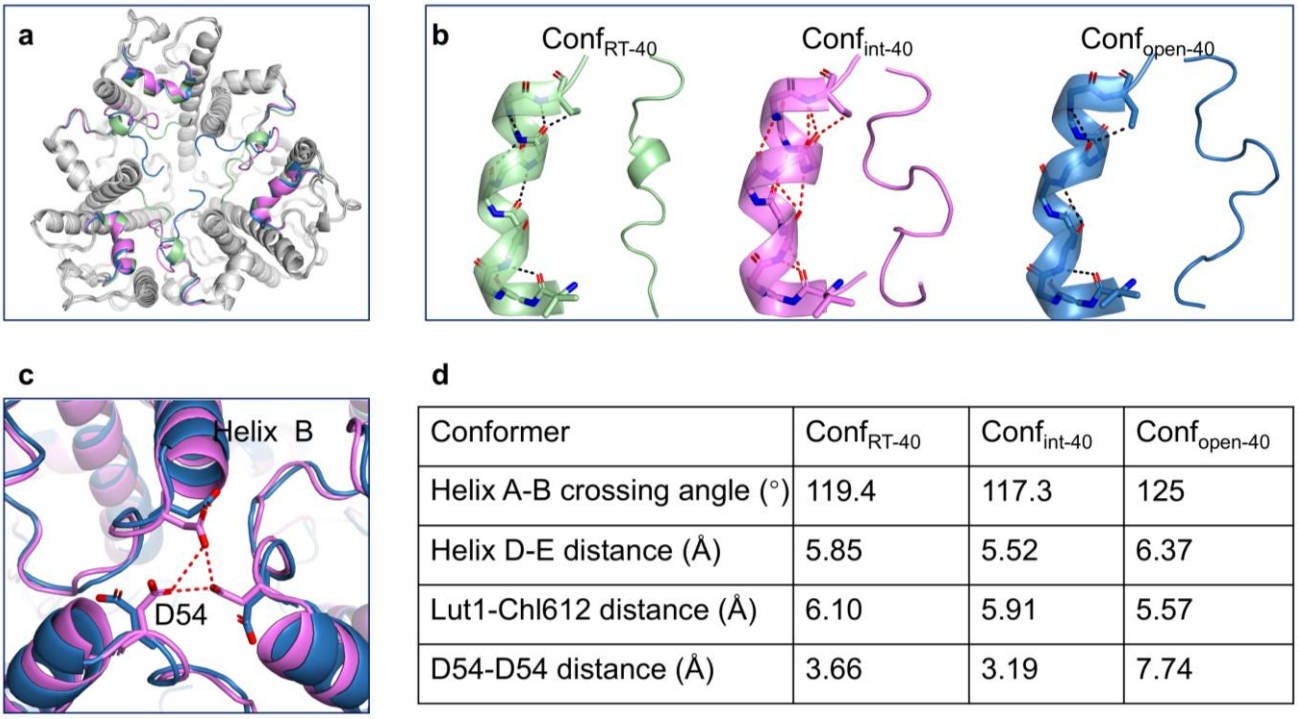

Conformer	Conf$_{RT-40}$	Conf$_{int-40}$	Conf$_{open-40}$
Helix A-B crossing angle (°)	119.4	117.3	125
Helix D-E distance (Å)	5.85	5.52	6.37
Lut1-Chl612 distance (Å)	6.10	5.91	5.57
D54-D54 distance (Å)	3.66	3.19	7.74

Extended Data Fig. 12: Structural analysis of conformers at 40 °C. (a) Lumenal-view structural alignment of three LHCII conformers resolved at 40 °C, Conf$_{RT-40}$ in green, Conf$_{int-40}$ in violet, Conf$_{open-40}$ in blue. (b) Detailed secondary structure comparison of helix E (left) and C-terminal (right) between three varied LHCII conformers at 40 °C. (c) Formation and disruption of the hydrogen bond network among D54 of each monomer in Conf$_{int-40}$ and Conf$_{open-40}$. (D) Structural parameters of LHCII conformers at 40 °C.

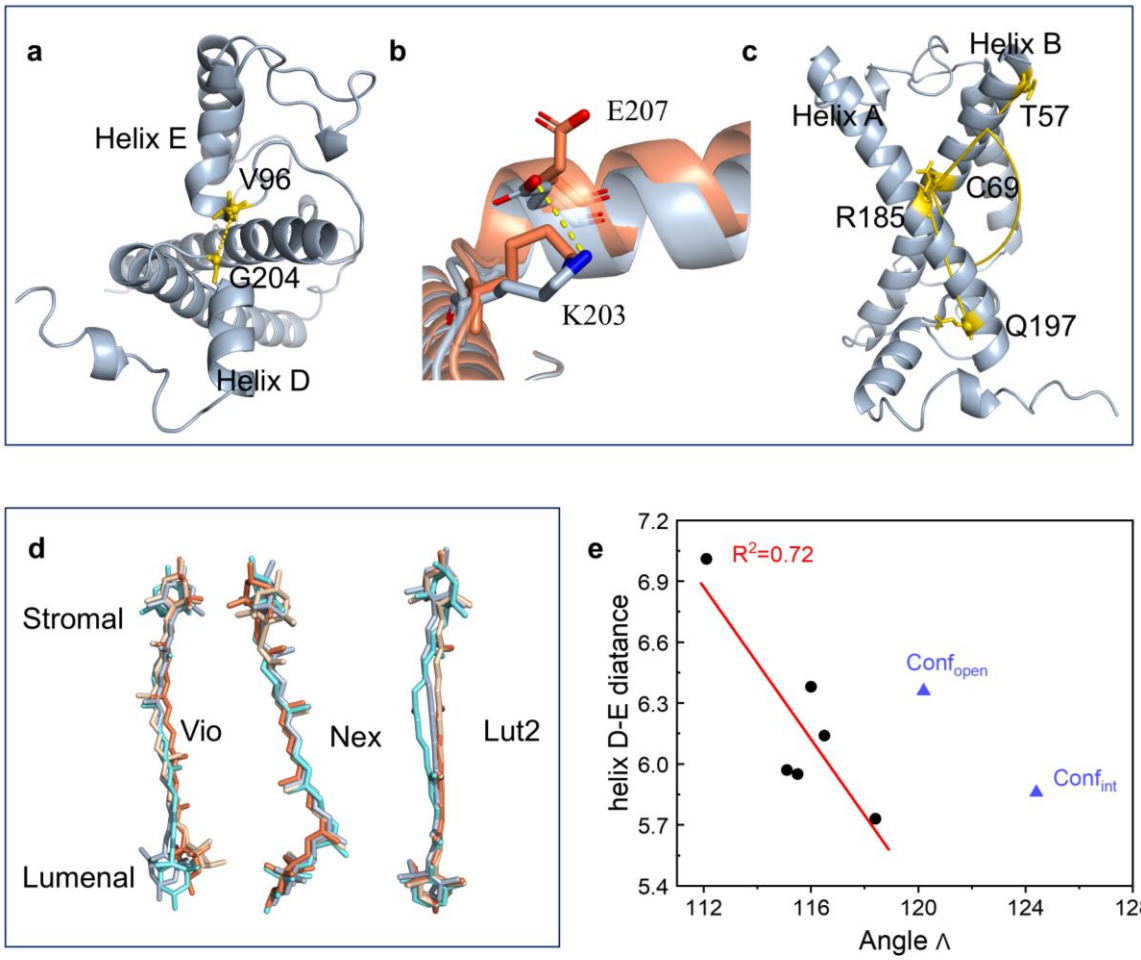

Extended Data Fig. 13: Schematic diagram of structural parameter definition, and pigments alignment comparison. (a) Helix D-E distance defined by the distance between the Cα of residues V96 and G204. (b) Rearrangement of K203 and E207 at the lumenal side in $Conf_{RT}$ and $Conf_{close}$, with yellow dashed lines marking salt-bridge formation between K203 and E207 in $Conf_{RT}$. (c) LHCII monomer of Conf1 represents the helix A-B angle (left) defined by the dihedral angle of the Cα of residues T57-C69-R185-Q197. (d) Alignments comparison of Vio, Nex, and Lut2 in four conformers at 55 ℃, $Conf_{RT}$ in lightSteelBlue, $Conf_{int}$ in peachPuff, $Conf_{close}$ in coral, and $Conf_{open}$ in cyan. (e) The relationship between the angle Λ and the helix D-E distance in varied conformers. Data are derived from $Conf_{RT}$, $Conf_{closed}$, unprotonated and protonated LHCII in detergent or LHCII nanodisc (PDB ID: 8IWX, 8IWY, 8IX0, 8IX1). The angel Λ is defined by the angle of Cα atoms of E207, D211, and N223, the red line is linear fitting result of the black dots. For $Conf_{int}$ and $Conf_{open}$ (triangles), Λ increases greatly to 127.3° and 120.6° due to the disordering of the C-terminal structure, thus Λ in $Conf_{int}$ and $Conf_{open}$ don't conform to the linear relationship.

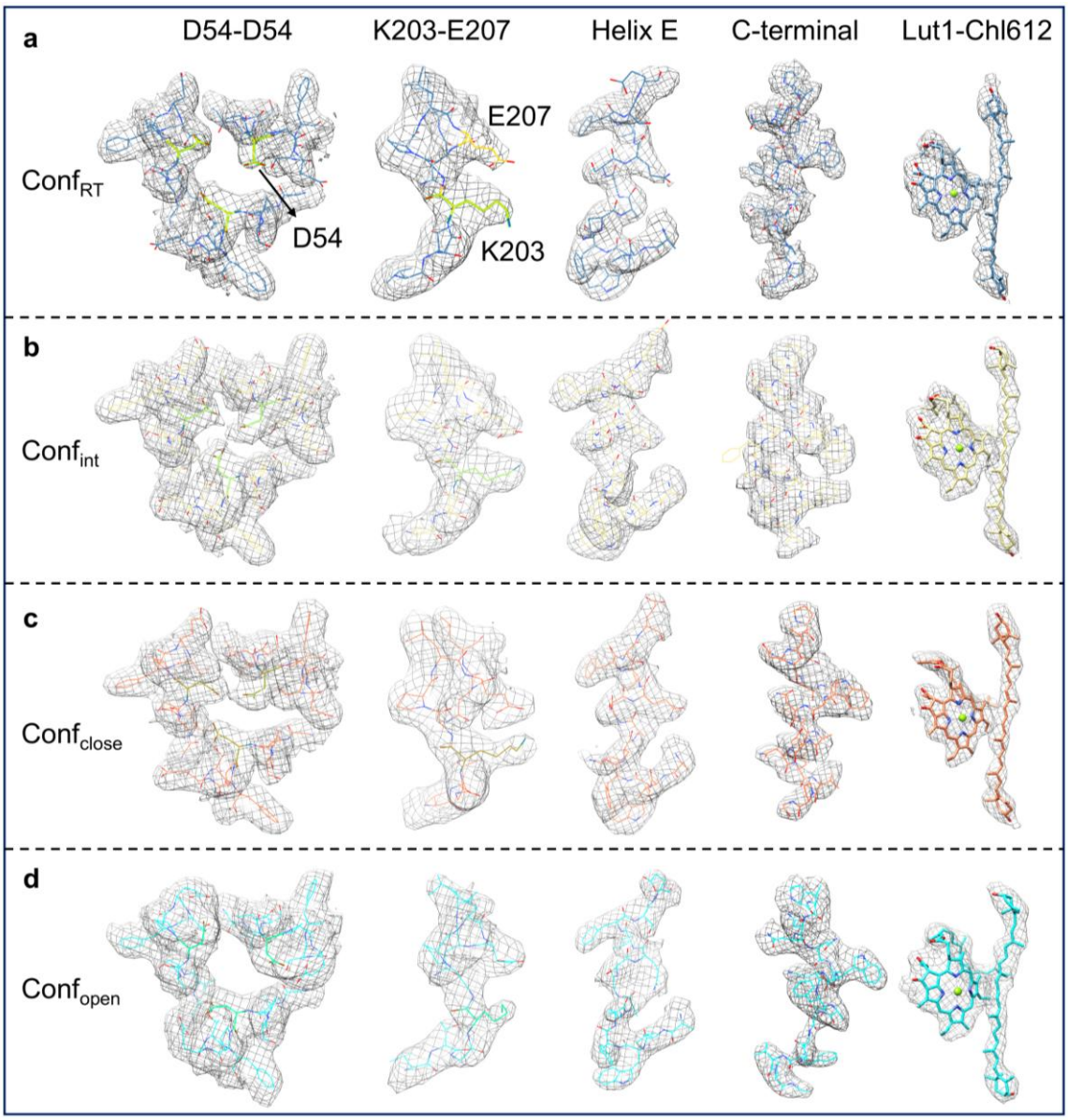

Extended Data Fig. 14: Electron-density map of local secondary structures and pigments of the four conformations at 55 °C. The density map of the D54-D54 interaction between three monomers, K203-E207, helix E, C-terminal, and Lut1-Chl612 pigment pair in Conf$_{RT}$ (a), Conf$_{int}$ (b), Conf$_{close}$ (c), and Conf$_{open}$ (d).

Temperature	40 ℃			55 ℃			
Conformations	$Conf_{RT-40}$	$Conf_{int-40}$	$Conf_{open-40}$	$Conf_{RT}$	$Conf_{int}$	$Conf_{closed}$	$Conf_{open}$
PDB Code	22MA	22MB	22IN	22IM	22IL	22IJ	22IC
Data collection and processing							
Voltage (kV)	300			300			
Electron dose ($e^-/Å^2$)	50			50			
Defocus range (μm)	-1.0 to -2.0			-1.0 to -2.0			
Pixel size (Å)	0.85 Å			0.85 Å			
Symmetry imposed	C1			C1			
Number of images	11,098			16,159			
Number of total particles	14,756,164			22,127,598			
Number of used particles	254,411	392,268	55,653	418,984	984,545	565,561	651,914
Map resolutions (Å) (FSC 0.143)	2.91	2.84	3.21	2.95	2.61	2.74	3.06
Refinement							
Initial model used (PDB code)	1RWT			1RWT			
B factors ($Å^2$)							
Protein	37.43	33.34	47.14	29.66	23.83	19.83	35.42
Ligand	38.05	33.29	48.72	28.94	23.65	19.69	36.59
R.m.s. deviations							
Bond length (Å)	1.405	1.373	1.882	1.521	1.456	1.295	1.705
Bond Angle (°)	0.006	0.009	0.015	0.007	0.009	0.006	0.012
Validation							
MolProbity score	1.82	1.81	1.78	1.78	1.88	1.80	1.88
Clashscore	11.34	9.48	8.03	10.99	10.21	9.79	9.72
Poor rotamers (%)	0	0.20	0.40	0	0.60	0.79	0.60
Ramachondran plot							
Favored (%)	96.30	95.52	95.06	96.60	94.91	95.83	94.60
Allowed (%)	3.70	4.48	4.94	3.40	5.09	4.17	5.40
Disallowed (%)	0	0	0	0	0	0	0

Extended Data Table 1: Cryo-EM data collection, refinement and validation statistics of LHCII structures at two different temperatures.

Temperature	25 °C	55 °C			
Conformations	\	$Conf_{RT}$	$Conf_{int}$	$Conf_{close}$	$Conf_{open}$
PDB Code	8IWX	22IM	22IL	22IJ	22IC
Fluorescence lifetime (ns)	3.52	2.14			
Lut1-Chl612 distance (Å)	5.99 (0.03)	6.06 (0.02)	5.93 (0.16)	5.94 (0.31)	5.47 (0.06)
Helix D-E distance (Å)	5.95 (0.03)	5.97 (0.06)	5.86 (0.48)	5.73 (0.10)	6.36 (0.06)
Helix A-B crossing angle (°)	119.3 (0.6)	118.8 (0.4)	117.1 (1.6)	118.0 (1.0)	124.4 (1.8)
Angle Λ (°)	115.5 (0.1)	115.1 (1.1)	124.4 (1.4)	118.4 (1.4)	120.2 (2.6)
Angle Γ (°)	94.2 (1.0)	94.0 (0.8)	92.0 (1.7)	89.4 (0.4)	99.3 (0.9)
Helix E state	3_{10}-helix	3_{10}-helix	α-helix	α-helix	3_{10}-helix
C-terminal state	Random coil	Random coil	Random coil [a]	α-helix	Random coil [a]
D54-D54 distance (Å)	5.15 (0.68)	5.16 (0.46)	3.35 (0.31)	3.52 (0.69)	7.90 (0.07)
K203-E207 distance (Å)	4.04 (0.26)	4.44 (0.94)	4.55 (0.67)	5.90 (1.04)	8.58 (0.11)
Salt bridge (E65-R185)	3.56 (0.30)	3.35 (0.59)	2.91 (0.13)	3.16 (0.35)	2.69 (0.21)
Salt bridge (R70-E180)	3.61 (0.26)	3.82 (0.88)	3.02 (0.50)	3.80 (0.90)	2.80 (0.20)
Lut1-Chl612 coupling (cm^{-1})	32.3	30.4	58.9	51.7	196.4 (N)/575.7 (Y) [b]

Extended Data Table 2: Structural parameters for different LHCII conformers.

[a]: a more disorder random coil. [b]: Lut1-Chl612 coupling in Chain N and Chain Y. Data in bracket are the standard deviations of the average values.

References

1 Kelly, D., Franca, L. G., Stavrou, K., Danos, A. & Monkman, A. P. Laplace Transform Fitting as a Tool To Uncover Distributions of Reverse Intersystem Crossing Rates in TADF Systems. *Journal of Physical Chemistry Letters* **13**, 6981-6986 (2022).

2 Ruan, M. *et al.* Cryo-EM structures of LHCII in photo-active and photo-protecting states reveal allosteric regulation of light harvesting and excess energy dissipation. *Nat. Plants* **9**, 1547-1557 (2023).

3 Berera, R., van Grondelle, R. & Kennis, J. T. M. Ultrafast transient absorption spectroscopy: principles and application to photosynthetic systems. *Photosynth. Res.* **101**, 105-118 (2009).

4 Zheng, M., Pang, X., Chen, M. & Tian, L. Ultrafast energy quenching mechanism of LHCSR3-dependent photoprotection in Chlamydomonas. *Nat. Commun.* **15**, 4437 (2024).

5 Li, H. *et al.* Dynamical and allosteric regulation of photoprotection in light harvesting complex II. *Sci. China Chem.* **63**, 1121-1133 (2020).

6 Cupellini, L., Calvani, D., Jacquemin, D. & Mennucci, B. Charge transfer from the carotenoid can quench chlorophyll excitation in antenna complexes of plants. *Nat. Commun.* **11**, 662 (2020).

7 Daskalakis, V. *et al.* Structural Basis for Allosteric Regulation in the Major Antenna Trimer of Photosystem II. *J Phys Chem B* **123**, 9609-9615 (2019).

8 Pedraza-Gonzalez, L., Accomasso, D., Cupellini, L., Granucci, G. & Mennucci, B. Ultrafast excited-state dynamics of Luteins in the major light-harvesting complex LHCII. *Photochemical & Photobiological Sciences* **23**, 303-314 (2024).

9 Accomasso, D., Londi, G., Cupellini, L. & Mennucci, B. The nature of carotenoid S* state and its role in the nonphotochemical quenching of plants. *Nat. Commun.* **15** (2024).